Time domain approach to semiclassical dynamics: Breaking the log time barrier

Eric J. Heller, Steven Tomsovic, and Miguel A. Sepúlveda
Departments of Physics and Chemistry, BG-10, University of Washington, Seattle, Washington 98195

(Received 18 September 1991; accepted for publication 14 January 1992)

The presence of chaos in the classical dynamics is not necessarily the destructive element it was thought to be for semiclassical approximations in the time domain. The method of calculating the semiclassical propagation of initial states and correlation functions for nonlinear and chaotic dynamics is shown, and the excellent accuracy is noted for rather long times. The breakdown timescale is much longer than the infamous "log time" for the cases investigated here.

I. INTRODUCTION

Semiclassical mechanics provides both physical insight and approximations to a wide array of quantum mechanical problems. It began in the form of the "Old Quantum Theory" as an approximate quantization scheme. The Van Vleck Green's function expression solidifies the Old Quantum Theory and dates to 1928.[1] In many ways, the study of the formal, general structure of the semiclassical limit culminated with the rigorous mathematical framework constructed by Maslov and Fedoriuk[2] and the derivation of semiclassical trace formulas by Gutzwiller[3] 20 to 25 years ago. Yet, in spite of the formal developments, the subject cannot be said to be in a satisfactory state. Even the conditions under which semiclassics provides a good approximation are poorly understood. The perspective on such longstanding problems differs according to whether one studies the time or the energy Green's functions. Many of the still unresolved problems in semiclassical theory are naturally attacked in the time domain, which traditionally has received relatively less attention than the energy domain. In fact, even the techniques for evaluating the semiclassical time propagator have, until recently, remained in a quite primitive state.

A crucial issue is the time interval over which semiclassical propagation tracks the quantum evolution of an initial state, and especially whether or in what way the nature of the underlying classical dynamics plays a role. Little existing work is published on this subject beyond Refs. 4 and 5, to which we shall return in Sec. II.

If the underlying dynamics are integrable, semiclassics typically provide excellent approximations to spectra and eigenstates. However, systems far from integrability, having either mixed phase space dynamics or being fully chaotic, present a number of ongoing theoretical challenges. The most important energy domain approaches fall into the category of periodic orbit theories, as embodied in the work of Gutzwiller.[3,6] They extract spectral information from the knowledge of the classical periodic orbits; some efforts along these lines to infer eigenstate properties also exist; see the work of Bogomolny[7] and Ozorio de Almeida.[8] Attempts to reproduce detailed spectra in the chaotic regime have proven difficult, but are experiencing a resurgence.[9] Justification of these techniques is still unclear[10] and should ultimately be linked to the validity of the dynamical approximation.

Surprisingly, it seems that the time-dependent semiclassical Green's function has been more or less ignored, with the notable exceptions of Refs. 4 and 5 and the original discussion of eigenstate scarring by the shortest periodic orbits.[11] The semiclassical propagator has never been systematically tested for a system far from integrability—the time scale of its validity is quite unknown. One reason for its being overlooked may be a deep-rooted, intuitive pessimism about the approximation's applicability, since the nonzero size of Planck's constant must be responsible for some kind of smoothing over the intricate complexity that is the essence of chaotic dynamics (or the intricate coexistence of regular and chaotic motion found in mixed systems). This intuition would suggest that space structures on a scale much finer than h cannot be relevant, and, once a time scale is reached where the chaos is well developed, the approximation ceases to function. A typical argument stresses, for example, that it is easy to find a perturbation which, though barely affecting the quantum system, radically alters each of the classical trajectories—the Correspondence Principle is failing. A further explanation of this gap lies in the technical difficulty of evaluating the formal semiclassical expression. In this article, we shall outline two methods that we have developed for performing the evaluation and demonstrate the astonishingly quantitative agreement existing between the quantum and semiclassical dynamics for systems with nonintegrable underlying dynamics. The first application is to an integrable system. Next, we treat a system with a smooth polynomial potential possessing a mixed phase space structure. Third, we examine the stadium billiard which is purely chaotic. It is shown that the agreement extends well past the time that the chaos is highly developed and classical structure far finer than a quantum cell is put into the semiclassics. In the following, Secs. II A–II D were based on the work of Heller[12] and Heller and Sepulveda,[13] and Sec. III on the work of Tomsovic and Heller.[14]

II. SEMICLASSICAL PROPAGATION

A. The semiclassical Green's function

Our starting point is to consider the quantum mechanical, time-dependent Green's function in a coordinate representation. It is denoted

$$G(\mathbf{q},\mathbf{q}';t) = \langle \mathbf{q}|e^{-i\hat{H}t/\hbar}|\mathbf{q}'\rangle, \tag{1}$$

where $\hat{H}$ is a quantum Hamiltonian. The propagation of an initial state $\Phi(\mathbf{q};0)$ is then given as

$$\Phi(\mathbf{q};t) = \int_{-\infty}^{\infty} d\mathbf{q}'\, G(\mathbf{q},\mathbf{q}';t)\Phi(\mathbf{q}';0). \tag{2}$$

The semiclassical propagation of a wave function parallels Eq. (2), with the Green's function replaced by its semiclassical form:[1–3]

$$\begin{aligned} G(\mathbf{q},\mathbf{q}';t) &\approx G_{sc}(\mathbf{q},\mathbf{q}';t) \\ &= \left(\frac{1}{2\pi i\hbar}\right)^{d/2} \sum_j \left|\mathrm{Det}\left(\frac{\partial^2 S_j(\mathbf{q},\mathbf{q}';t)}{\partial \mathbf{q}\partial \mathbf{q}'}\right)\right|^{1/2} \\ &\quad \times \exp(iS_j(\mathbf{q},\mathbf{q}';t)/\hbar - i\pi\nu_j/2). \end{aligned} \tag{3}$$

In this expression, the sum over j is for all trajectories connecting $\mathbf{q}'$ to $\mathbf{q}$ in time t, d is the number of degrees of freedom; the determinant is playing the role of the square root of a classical probability, and the phase is determined by the classical action $S_j(\mathbf{q},\mathbf{q}';t)$ and an index based on the properties of the conjugate points (like focal points), ν_j. $S_j(\mathbf{q},\mathbf{q}';t)$ is specified by the time integral of the Lagrangian $\mathcal{L}$:

$$\begin{aligned} S_j(\mathbf{q},\mathbf{q}';t) &= \int_0^t dt'\, \mathcal{L} \\ &= \int_0^t dt'\{\mathbf{p}(t')\cdot\dot{\mathbf{q}}(t') - H(\mathbf{p}(t'),\mathbf{q}(t'))\} \end{aligned} \tag{4}$$

along the jth classical path (H is the classical Hamiltonian). We have been calling Eq. (3) the Van Vleck propagator, although it was Gutzwiller[3] who, much later, added the ν_j index. Within the realm of semiclassical techniques,[15] the integral in Eq. (2) would normally be done by stationary phase. Given the Green's function, $G_{sc}(\mathbf{q},\mathbf{q}';t)$, one has the option of doing the integral by some other means. However, if the initial state is a Gaussian and the integral is done by stationary phase, we are forced to confront the issue of classical trajectories with complex initial conditions in real time; see the description of generalized Gaussian wave packet dynamics in Ref. 16. We avoid such complications using the theory described here.

Although Eq. (3) formally gives the semiclassical dynamics, as it stands it is prohibitively complicated to calculate as trajectories of all energies, and complexity must be incorporated. In addition, $G_{sc}(\mathbf{q},\mathbf{q}';t)$ suffers from a proliferation of singularities in the determinant prefactor due to the coalescence of stationary phase points associated with caustics (a generalization of classical turning points).[4] Our approach to avoiding these difficulties begins with applying $G_{sc}(\mathbf{q},\mathbf{q}';t)$ to the propagation of initially localized wave packets, $\Phi(\mathbf{q};0)$, of the form

$$\Phi(\mathbf{q};0) = (\pi\sigma^2)^{-d/4}\exp\left(-\frac{(\mathbf{q}-\mathbf{q}_0)^2}{2\sigma^2} + \frac{i\mathbf{p}_0}{\hbar}\cdot(\mathbf{q}-\mathbf{q}_0)\right). \tag{5}$$

The centroid $(\mathbf{q}_0,\mathbf{p}_0)$, determines the region of phase space around which the wave packet is localized. The shape of this region can be roughly visualized by taking the Wigner transform of Eq. (5), which is a Gaussian distribution centered at $\mathbf{q}_0,\mathbf{p}_0$ with $\Delta x^2 = \sigma^2$, $\Delta p^2 = (\hbar/\sigma^2)$. In wave packet propagation, the singularities of $G_{sc}(\mathbf{q},\mathbf{q}';t)$ in $\mathbf{q}'$ for fixed $\mathbf{q}$ are largely integrated out[17] in the course of the $d\mathbf{q}'$ integration. Further, only trajectories within some energy window will be relevant, thus vastly simplifying the orbits that need to be calculated. The specific Gaussian form has been chosen mostly for convenience and it is not essential; any smooth, square integrable functions would do. There is the additional motivation of experiments in atomic and molecular physics where initial Gaussian wave packets are approximately realizable.

B. Cellular dynamics

There are still an uncountable number of complicated contributing orbits if Eq. (3) is applied to the propagation of a Gaussian wave packet: all those with initial position $\mathbf{q}$ and initial momentum $\mathbf{p}$ "within" the Gaussian. We address this problem with two steps. First, the semiclassical Green's function is rewritten in a new form which emphasizes the contribution of individual trajectories in coordinate space, each with an amplitude and a phase:

$$\begin{aligned} G_{sc}(\mathbf{q},\mathbf{q}';t) = \left(\frac{1}{2\pi i\hbar}\right)^{d/2} \int d\mathbf{p}'\, \delta(\mathbf{q}-\mathbf{q}_t)\|J\|^{-1/2} \\ \times \exp[iS(\mathbf{q},\mathbf{q}';t) - i\pi\nu(\mathbf{q}',\mathbf{p}')/2], \end{aligned} \tag{6}$$

where

$$\|J\| = \left|\mathrm{Det}\left(\frac{\partial^2 S(\mathbf{q},\mathbf{q}';t)}{\partial \mathbf{q}\,\partial \mathbf{q}'}\right)\right|. \tag{7}$$

Several things need to be said about Eq. (6). For each $\mathbf{q}'$, there is an integral over initial $\mathbf{p}'$, and the final position $\mathbf{q}_t(\mathbf{q}',\mathbf{p}')$ is a function of initial $(\mathbf{q}',\mathbf{p}')$. The sum over j is gone; each of the contributing terms j is recovered when, for some initial momentum $\mathbf{p}'$, the condition $\mathbf{q} = \mathbf{q}_t(\mathbf{q}',\mathbf{p}')$ is satisfied. The phase correction $\pi\nu(\mathbf{q}',\mathbf{p}')/2$ is a function of the initial conditions, and the determinantal prefactor is the inverse of that appearing in Eq. (3). This formula has a picturesque interpretation. The delta function is a trajectory in coordinate space, and the remainder of the expression constitutes the amplitude and the phase of the trajectory. The evolving Green's function is an integral over all trajectories leaving position $\mathbf{q}'$, each with a different velocity.

However, there are still an infinite number of momenta to integrate over, unless one wants to search laboriously for

the finite number of conditions $\mathbf{q}=\mathbf{q}_t(\mathbf{q}',\mathbf{p}')$, which would have to be done anew for each new $\mathbf{q}'$ (this is sometimes called the "root search"). If the root search is to be avoided, and still a finite number of trajectories are to be run, something additional is needed. The idea, introduced in Ref. 12 is to divide the phase space of initial conditions into cells, whose volume is completely flexible. The volume is to be made small enough that the classical dynamics can be linearized within the cell. The linearization means that the action S is expanded to second order, and positions and momenta are expanded to first order in the variation of the initial $\mathbf{q}',\mathbf{p}'$ about the center of each cell. The introduction of the cells is the second step, resulting in a finite number of trajectories needed to propagate a wave function.

A very convenient way of cellularizing phase space is to introduce Gaussian cells in the classical phase space of initial conditions. These cells overlap in such a way as to give a smooth unit density in phase space. The cells are arranged so that

$$\sum_{n,m} g_{n,m}(\mathbf{q}',\mathbf{p}') = \xi \sum_{n,m} \exp[-(\mathbf{p}'-\mathbf{p}_m)\cdot\mathscr{B}\cdot(\mathbf{p}'-\mathbf{p}_m) - (\mathbf{q}'-\mathbf{q}_m)\cdot\mathscr{A}\cdot(\mathbf{q}'-\mathbf{q}_m)] \approx 1, \quad (8)$$

n,m being sets of N integers that specify the centers $(\mathbf{q}_n,\mathbf{p}_m)$ of each $g_{n,m}$ in the $2N$-dimensional phase space; $\mathscr{A}$ and $\mathscr{B}$ are two $N\times N$ diagonal matrices depending on real parameters $(\alpha_1,\ldots,\alpha_N)$ and $(\beta_1,\ldots,\beta_N)$, respectively, which define the widths of the Gaussians (the α's will be usually taken equal; the same for β's); ξ is a normalization constant.

In propagating a wave function, the Green's function is applied to an initial state

$$\begin{aligned}\Phi(\mathbf{q}';t) &= \eta \int d\mathbf{q}'\, d\mathbf{p}'\, \delta(\mathbf{q}-\mathbf{q}_t)\|J\|^{1/2} \\ &\quad\times\exp[iS/\hbar - i\nu\pi/2]\Phi(\mathbf{q}';0) \\ &\approx \eta\xi \sum_{n,m} \int d\mathbf{q}'\, d\mathbf{p}'\, \delta(\mathbf{q}-\mathbf{q}_t)\|J\|^{1/2} g_{n,m} \\ &\quad\times\exp[iS/\hbar - i\nu\pi/2]\Phi(\mathbf{q}';0), \quad (9)\end{aligned}$$

$\eta=(2\pi i\hbar)^{-d/2}$.

The parameters α's and β'a will be taken large enough so that $g_{n,m}(\mathbf{q}',\mathbf{p}')$ is zero everywhere but near the center of the Gaussian. Under that assumption, we can now expand $S(\mathbf{q}',\mathbf{p}';t)$ and $\mathbf{q}_t(\mathbf{q}',\mathbf{p}')$ about $(\mathbf{q}_n,\mathbf{p}_m)$ and perform each of the integrals appearing in Eq. (9) separately; the result (see Ref. 12 for more details) is that the wave function $\Phi(\mathbf{q};t)$ is expressed as a sum of Gaussians

$$\Phi(\mathbf{q};t) = \eta\xi \sum_{n,m} G_{n,m}(\mathbf{q}), \quad (10)$$

whose Gaussian parameters in each $G_{n,m}(\mathbf{q})$ are determined by the linearized classical dynamics. The important fact is that only the trajectories at the cell centers need be run, together with the usual monodromy matrix information. No root searching is needed, and the problem has been reduced to a finite number of trajectories. As the cells are made smaller, more of them are needed, and Eq. (9) approaches the exact Van Vleck expression, Eq. (3).

Since the initial state, $\Phi(\mathbf{q}';0)$, is localized in some region of phase space, it will not be necessary to place trajectories in the entire $\{\mathbf{q}',\mathbf{p}'\}$ space because the integral over $\mathbf{q}'$ will annihilate their contribution; only trajectories placed in the region covered by $\Phi(\mathbf{q}';0)$ (in the sense of a Wigner representation) are relevant. The actual number of trajectories needed to perform the calculation up to time t depends on the stability of the system. The more unstable, larger will be the stretching of initial distances in phase space and larger will be the number of trajectories (cells) necessary to represent accurately the folds in the final Lagrangian manifold in phase space. In the first nonintegrable example to follow, the chaos is weak enough that the cellular method can be used directly in a four-dimensional phase space. However, for the strong chaos in the stadium billiard, a new method had to be invented that takes advantage of the structure of phase space for an unstable system.

C. An integrable potential

We consider a simple one-dimensional (but anharmonic) system as a first test of the efficacy of the Van Vleck Green's function propagation.[12] The dynamics is nonlinear, and shearing in phase space occurs, although just linearly with time. The Morse oscillator Hamiltonian we use is of the form

$$H=(p^2/2)+D[1-\exp(-\lambda q)]^2, \quad (11)$$

and the initial wave function is taken to be a single Gaussian of the form

$$\Phi(q,0)=(2\alpha/\pi)^{1/4}\exp[-\alpha(q-q_0)^2]. \quad (12)$$

Because of the nonlinearities, there is no *a priori* reason why we should expect the Van Vleck Green's function propagation to be accurate at long times (several or more vibrational periods of the oscillator). Because we use a single initial Gaussian, the cellular expansion over positions is not needed. For Fig. 1, we used 60 Gaussians equally spaced in momentum from -20 to 20. The Morse potential used had $D=160$, $\lambda=0.036$. The Gaussian had $\alpha=6.$, $q_0=2$. This makes a narrow Gaussian on the "soft" side of the potential. The "exact" quantum results were determined by fast Fourier transform. The time step for both the fast Fourier transform and trajectories for the semiclassical Green's function propagation was $\tau=0.02$. The wave function is plotted from $q=-12$ to $q=24.6$ in 128 increments of size 0.2857. This was the fast Fourier transform spatial step size as well. There is a large range of energies in the initial wave function so that the period is not well defined, but it is around $t=10$. In Fig. 1, the wave function is shown for approximately six periods. The left columns show the real part of the wave function, and the right columns show $|\Phi(q,t)|^2$. Except for small errors which sometimes accrue at turning points, the semiclassical wave function is remarkably accurate.

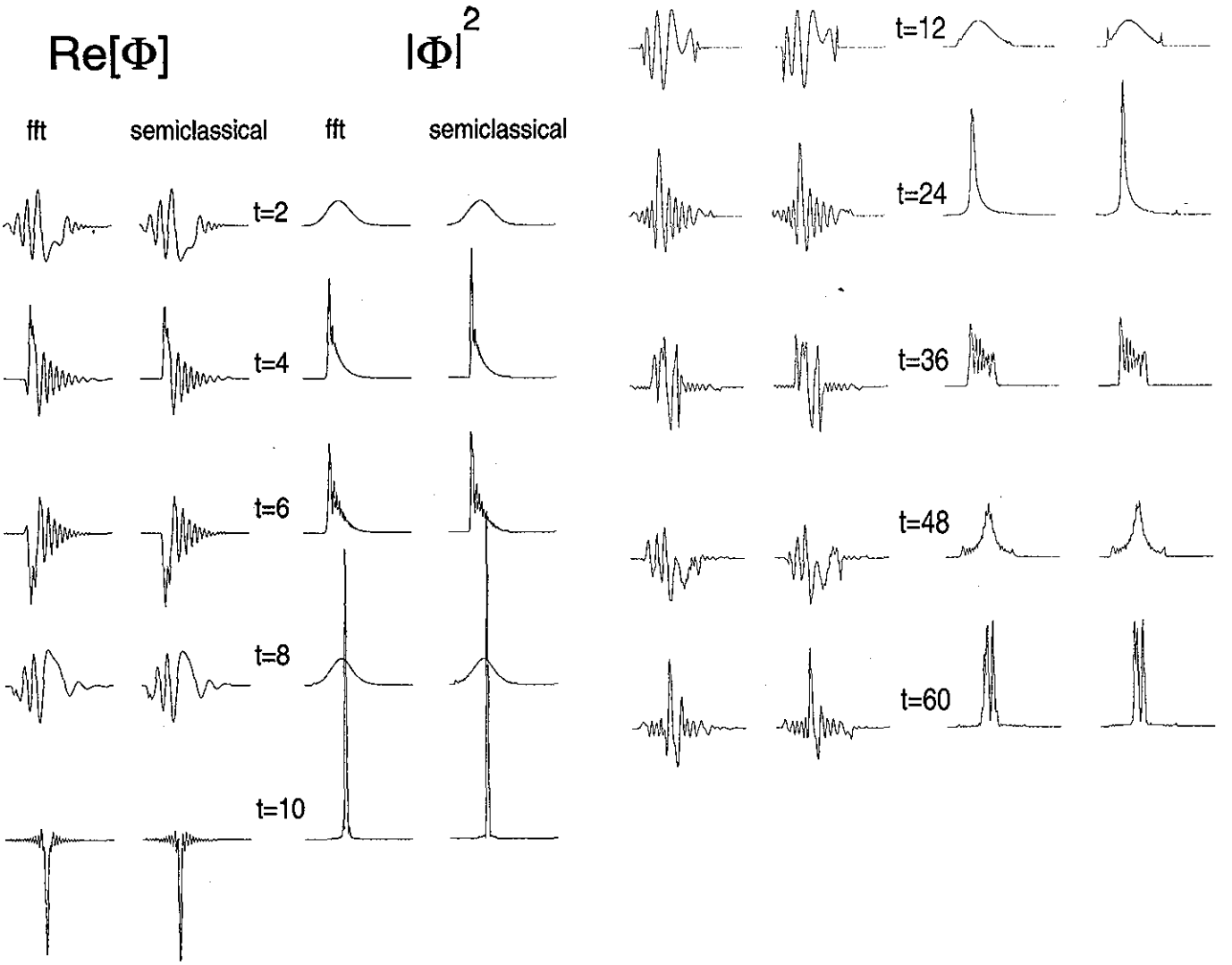

FIG. 1. Comparison of semiclassical cellular method results for $\Phi(q,t)$ and $|\Phi(q,t)|^2$ with numerical fast Fourier transform. The parameters are given in the text.

Next, we construct a spectrum out of the autocorrelation function:

$$S(E)\equiv\frac{1}{2\pi\hbar}\int_{-\infty}^{\infty}e^{iEt/\hbar}\langle\Phi(0)\,|\,\Phi(t)\rangle dt \tag{13}$$

$$=\frac{1}{2\pi\hbar}\sum_{n=0}^{\infty}|c_n|^2\int_{-\infty}^{\infty}e^{-i(E_n-E)t/\hbar}dt \tag{14}$$

$$=\sum_{n=0}^{\infty}|c_n|^2\delta(E_n-E). \tag{15}$$

We do this for the semiclassical wave function and the fast Fourier transform wave function. In the case of the fast Fourier transform, we found it necessary to take 512 points in order to converge the correlation function for the narrow initial Gaussian ($\alpha=5.$). The parameters were $q_0=2$, with $\alpha=6$ in the Morse potential with $D=30.$, $\lambda=0.08$. The time step was 0.01, and the total number of steps was 12 000. The correlation function was damped in both cases by a Gaussian with a form $\exp[-(t/40)^2]$. The correlation functions agreed very well. The spectrum results are shown in Fig. 2. This figure shows the excellent agreement on the intensities and the positions of the spectral peaks, including the correct anharmonic shift in the line spacings.

D. The Barbanis potential

Stepping up the complexity after the initial success in one dimension, we examine a two-dimensional system with soft chaos (i.e., a typical system) containing both quasi-integrable and chaotic domains in phase space. The two-dimensional Barbanis potential is typical of the anharmonic potential energy surfaces used in chemical physics to represent the vibration of polyatomic molecules. It is a very simple harmonic oscillator with an added cubic anharmonicity:

$$V(\mathbf{q})=\tfrac{1}{2}\omega_1^2q_1^2+\tfrac{1}{2}\omega_2^2q_2^2+\gamma q_1^2q_2. \tag{16}$$

We will take $\omega_1=1.1$, $\omega_2=1.0$, and $\gamma=-0.11$. Equipotential contours of the potential are shown in Fig. 3. The

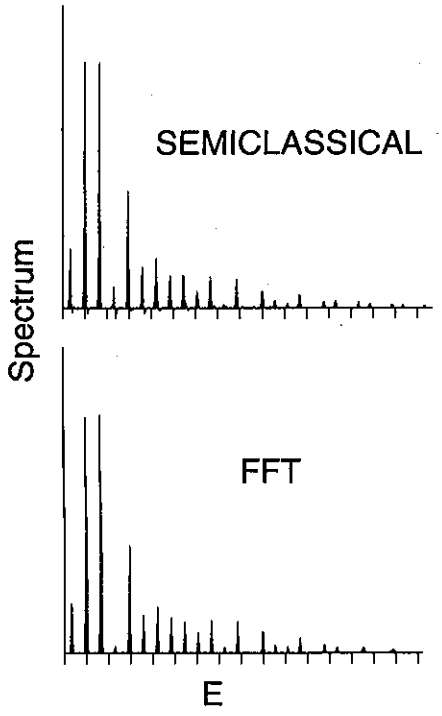

FIG. 2. Spectrum [Fourier transform of the autocorrelation function $\langle\Phi|\Phi(t)\rangle$] compared for the semiclassical and fast Fourier transform propagations. The parameters are given in the text.

full Hamiltonian is $H = \mathbf{p}^2/2 + V(\mathbf{q})$. Notice the existence of two dissociative channels in the potential.

The structure of phase space for this system is well studied, and the role of resonances, formation of local modes, onset of chaos, etc., are typical of many smooth Hamiltonian systems.[8] We will not examine these details here, but simply use the potential as a "typical" Hamiltonian system possessing soft chaos.

Our main focal point in what follows will be the autocorrelation function

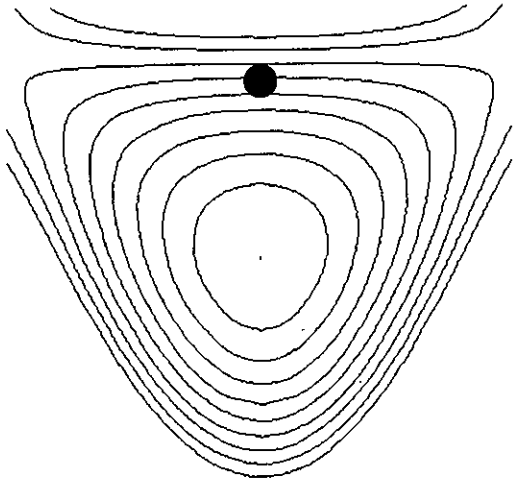

FIG. 3. Contours of the potential of Eq. (16), and an initial nonstationary wave packet.

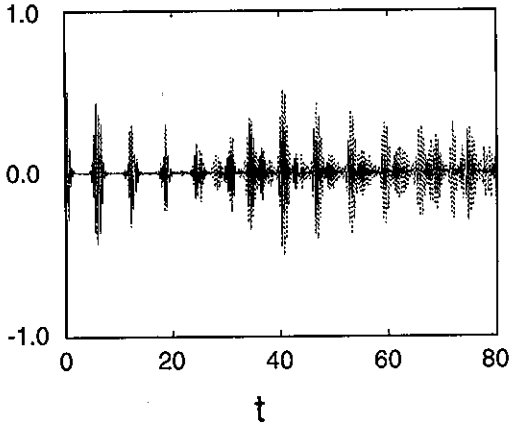

FIG. 4. Real part of $C(t)$. The dash line represents the quantum mechanical (FFT) result and the solid line the semiclassical Van Vleck Green's function propagation.

$$C(t) = \langle\Phi(0)|\Phi(t)\rangle, \tag{17}$$

which describes the dynamical evolution of the system and leads to the determination of the energy spectrum through Eq. (13).

We launch an initially Gaussian wave packet of the form

$$\Phi(\mathbf{q}) = (4\alpha_1\alpha_2)^{1/2}/\pi \exp[-\alpha_1 q_1^2 - \alpha_2(q_2 - 5)^2], \tag{18}$$

where $\alpha_1 = 3.3$ and $\alpha_2 = 3$. Considered in the basis of the uncoupled harmonic part of the potential, this nonstationary state consists of the ground state of the mode q_1, and series a highly excited states of the mode q_2. The real part of the quantum $C(t)$ is shown in Fig. 4.

Initially, as the wave packet moves away from position (0,5), there is a decay of the real part of the correlation function, with oscillations due to our choice of zero of energies. The magnitude of the correlation function decays as well. The Fourier transform of this first decay in $C(t)$ gives the envelope of the spectrum defined in Eq. (13). For our choice of $\Phi(0)$, the spectrum covers an energy range from $E = 8$ to 24. (For reference, the dissociation energy is approximately 15.125). A series four recurrences of period $\tau \approx 2\pi$ follows the initial decay in $C(t)$, with decaying amplitude. The period corresponds to the quasi-one-dimensional motion along q_2, the decay is a result of the q_1, q_2 coupling, which pushes energy and amplitude into the q_2 coordinate at the expense of q_1. In fact, a significant part of the high energy components of Φ dissociate after one bounce on the potential wall, i.e., after the first recurrence. Indeed, if we would Fourier transform the $C(t)$ after the first four recurrences, we would get the broadened spectrum of a 1-D harmonic oscillator.

Later, at $t \approx 30$, we observe the first nonlinear recurrence of the correlation function. By "nonlinear recurrence," we mean a recurrence due to amplitude that has left the $q_2 \approx 0$ region and come back. (The linearized dynamics of this oscillator brings escape from the line $q_1 \approx 0$ without return.) By this time the wave function looks to-

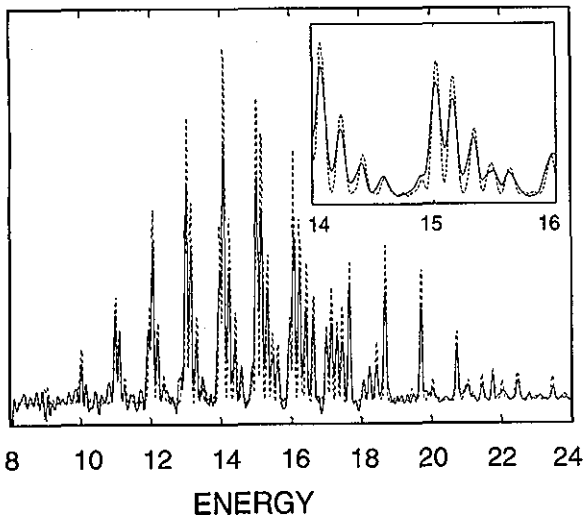

FIG. 5. The spectrum (numerical FFT of the autocorrelation function) of the initial wave packet discussed in the text, comparing the exact quantum result (FFT) and the semiclassical Van Vleck Green's function propagation. A detail is also shown.

tally delocalized in the bounded zone of the potential. This first nonlinear recurrence seems to be associated with low energy components.

Some of the components with energy well above dissociation continue very anharmonic oscillation in the bound region before escaping through the dissociation channels. This induces a series of aperiodic recurrences in $C(t)$.

We show the correlation function until time $t = 80$ in order to give the flavor for the dynamical nature of the system. The spectrum of Φ was also calculated and is shown in Fig. 5. Notice that the average energy is about 16 and that most of the initial state is above the dissociation threshold. There are also very sharp peaks between $E = 20$ and 24 that are related to resonances in the continuum.

Let us now turn to study the classical dynamics underlying the more or less typical example of quantum dynamics so far described. We first locate the Gaussian wave packet in phase space by looking at the width of the initial Gaussian $\Phi(0)$ both in coordinates and in momentum representation. In Fig. 6 we show two Poincaré surfaces of section that reveal the chaotic nature of the dynamics at energies close to the dissociation limit. The classical dynamics in the energy range 8–12 is mostly regular, showing that chaos is restricted to a narrow region of phase space. However, there are island chains in the phase space, corresponding to high-order resonances, so the dynamics is not trivial at lower energy either. There are also regions of quasi-integrable motion coexisting with the chaotic ones close to dissociation.

FIG. 6. Poincaré section of the Barbanis potential dynamics of $q_2 = 5$, $p_2 \geqslant 0$ at energy $E = 14$ (left) and $E = 15$.

The cellular dynamics method described in Sec. II B was used to calculate the semiclassical autocorrelation function. A total of 52 855 cells were located in phase space around the center of the Gaussian; each one had a volume 0.11 339. Only 18 186 trajectories were in the energy range $8 \rightarrow 24$; the others are not run. By $t = 20$, 15 500 remained undissociated; at $t = 60$, only $\approx 12\,000$ remained. The guiding trajectories were distributed between the quasi-integrable and chaotic regions. No attention was given to their relative importance with respect to the $C(t)$ to be calculated; some trajectories contribute more than others. Also, special care had to be taken to calculate the shift in the phase ν of Eq. (9). The details of this calculation will be given elsewhere.[13]

Figure 4 also shows the semiclassical $C(t)$. Notice that it not only describes, as expected, the linear recurrences but also the nonlinear ones arising after time $t = 30$. There is a small low-frequency discrepancy between quantum and semiclassical results that we believe is related to the fact that our calculation may still lack some important low-energy trajectories. Nevertheless, the success of semiclassics on handling this kind of system with such mixed dynamics is evident when we Fourier transform the full semiclassical autocorrelation function and compare it with the exact quantum mechanical one, in Fig. 5. Almost all of the states are resolved, specially the ones in the classically chaotic region; also the dissociative part of the spectrum is accurately represented by the semiclassical calculation.

The cellular method for the semiclassical propagation of a wave packet is in essence very simple: Find the region covered in phase space by the initially localized state, locate a sufficient number of trajectories in it, and integrate them forward in time in order to calculate the semiclassical wave function being propagated. No detailed knowledge about what is going on in classical phase space is necessary.

The number of trajectories needed to calculate $\Phi(t)$ up to time t may grow exponentially as the dynamical system becomes more chaotic. This is the price we have to pay for ignoring the nature of the dynamics and not sorting out which trajectories are relevant for the determination of $C(t)$ and which ones are not. As long as the dynamical system is not very chaotic, the cellular dynamics method can handle it fairly well; otherwise, an approach like the one presented in the following section is needed.

III. CHAOS AND UNEXPECTED LONG TIME ACCURACY

A. Stationary phase, the area-$\hbar$ rule and the log time

To date, the most extensive theoretical treatment of how chaos affects the stationary phase approximation is given in Ref. 4, where it was argued that the semiclassical

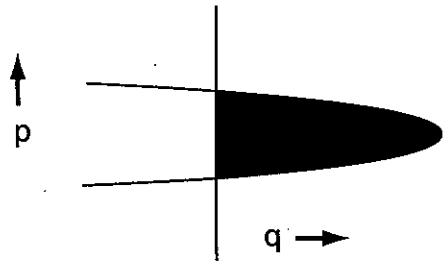

FIG. 7. The area contained between intersections of the time evolved manifold of a state and a position state (vertical line) is shown as black. If this area falls below $\hbar$, the semiclassical amplitude is in doubt.

evolution of a state under chaotic dynamics remains accurate only over an extremely short time scale, $t^* = O(\ln(\hbar^{-1}))$, which is dubbed the log time. The reasoning was that, by this time or soon thereafter, the problems with caustics become quite severe. The argument is as follows. The propagation of a quantum state is connected via semiclassics to the propagation of a manifold of trajectories. Assuming the dynamics are chaotic and bounded, the manifold will stretch out exponentially fast, depending on the Laypunov exponent, and then begin folding back upon itself. The time when folding is found everywhere cannot be delayed beyond the log time.

In the vicinity of a fold, the projection of the state into configuration space generally will have two nearby stationary phase points. Consider an isolated case of two coalescing stationary phase points, as illustrated in Fig. 7.

In this example, a uniformization of the simple stationary phase approximation leads to an accurate Airy function form whose argument depends on the black shaded region in the figure. If this area is large compared with $\hbar$, the leading asymptotic form of the Airy function is good and it recovers the nonuniformized sum of two isolated stationary phase points. If this area is of the order of $\hbar$ or smaller, the uniformization is essential. This is the "area-$\hbar$ rule" and it gives a rough idea of the domain over which a nonuniformized caustic leads to inaccuracies in the semiclassics. Once folds develop, they proliferate exponentially rapidly. So, although one might consider uniformizing a pair of isolated, coalescing stationary phase points, soon after the log time one would be overwhelmed by multitudes of coalescing points everywhere. The semiclassical approximation appears to be headed for a total collapse in this view. It was mentioned earlier that certain kinds of caustic problems that arise in $G_{sc}(\mathbf{q},\mathbf{q}';t)$ will not show up in the propagation of a smooth state. But that just implies that the picture painted here for a propagating state would be even worse if described for the Green's function. It certainly seems reasonable that chaos puts up a barrier at the log time against which semiclassics cannot easily penetrate.

B. Classical transport: heteroclinic orbit summations

Rigorous testing of the concept of the log time barrier presents some new practical challenges in evaluating the semiclassical propagator. To reach propagation times well beyond the log time necessarily means that, even very close neighboring initial conditions have "gone their separate ways." If one were by brute force to apply the cellular dynamics of Sec. II B, one would rapidly require thousands of trajectories per phase space dimension. Even with just two degrees of freedom, the computations would be beyond reach. One-dimensional quantum maps would provide a simpler testing ground than continuous dynamical systems, and work along these lines has been done with the quantum baker's map.[19] These maps tend to be somewhat abstract and here we have decided to concentrate on continuous systems. We need to both simplify the problem and find a more sophisticated approach. For simplification, we shall concentrate on correlation functions of the type

$$C_{ab}(t) = \langle \Phi_a(0) \,|\, \Phi_b(t) \rangle = \int_{-\infty}^{\infty} d\mathbf{q}\, d\mathbf{q}'\, \Phi_a^*(\mathbf{q};0) G(\mathbf{q},\mathbf{q}';t) \Phi_b(\mathbf{q}';0), \quad (19)$$

where $\Phi_a(\mathbf{q};0)$ and $\Phi_b(\mathbf{q};0)$ are wave packets of the form given in Eq. (5). Note that the correlation functions entail no loss of generality since all the information contained in $G(\mathbf{q},\mathbf{q}';t)$ is also contained in the full set of possible $C_{ab}(t)$. Next, we need to incorporate some of the known features of chaos. The cellularization of Sec. II B is general and was constructed in a "blind" fashion paying no attention to the nature of the system's dynamics. However, there is a lot of redundant information being calculated. Certain neighboring cells are related to each other, etc. Much of this can be accounted for from the beginning, assuming the system is chaotic.

The first task is to identify all those trajectories that will contribute to $C_{ab}(t)$ at time t precisely. The trajectories necessarily begin in the neighborhood of the centroid of $\Phi_b(0)$, $(\mathbf{q}_0,\mathbf{p}_0)_b$, and finish near the centroid of $\Phi_a(0)$, $(\mathbf{q}_0,\mathbf{p}_0)_a$. The procedure for locating trajectories is tantamount to solving the problem of calculating a classical version of $C_{ab}(t)$ where localized classical densities of phase points are used in lieu of wave packets. The details will be published elsewhere[20] and here we just roughly describe the main idea. Consider an initial classical density ρ_b which is propagated a time t and projected onto another density ρ_a to form a correlation function

$$\mathscr{C}_{ab}(t) = \langle \rho_a \rho_b(t) \rangle. \quad (20)$$

Assume ρ_a and ρ_b are chosen appropriately to correspond to Φ_a and Φ_b; here, they would be the Gaussians found in the Wigner transforms of Φ_a and Φ_b. Illustrated schematically in Fig. 8 are the principle features of chaos upon which we rely. Any initial density of phase points being propagated preserves its volume (Liouville's theorem), and the phase space has a local hyperbolic structure, meaning that nearby trajectories are either separating or approaching each other exponentially fast. An initially smooth, localized density rapidly evolves and becomes like the filamentary strand pictured. Assuming the accessible phase space is bounded, the filamentary density rapidly folds over upon itself with the number of "folds" proliferating exponentially in time. The intersection of the various branches of the filamentary density with the neighborhood of $(\mathbf{q}_0,\mathbf{p}_0)_a$ identifies the endpoints of all the trajectories

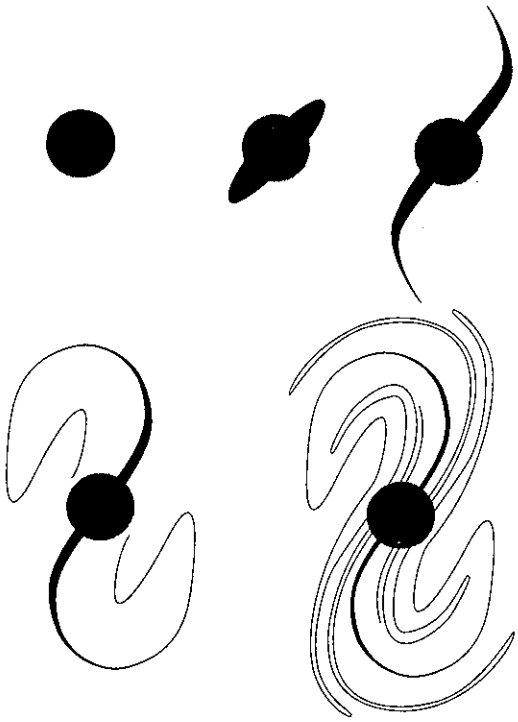

FIG. 8. A schematic illustration of the hyperbolic structure of phase space. The initial swarm of trajectories, the grey disk, exponentially stretches apart as time evolves from upper left to lower right.

contributing to $\mathscr{C}_{ab}(t)$; the initial conditions are easily found by following the trajectories backward.

The trajectories are naturally grouped into subsets labeled by the branch in which their endpoints reside. All the trajectories within a particular subset are exceedingly similar in their properties and its suffices to locate a single member within a branch in order to understand the behavior of all the members of a subset. For a system with two degrees of freedom, it is a simple matter to locate the one reference trajectory per subset referred to as being "heteroclinic" to the classical points $(\mathbf{q}_0,\mathbf{p}_0)_b$ and $(\mathbf{q}_0,\mathbf{p}_0)_a$.[20] Briefly, these heteroclinic points lie at the intersection of the unstable manifold associated with $(\mathbf{q}_0,\mathbf{p}_0)_b$ and the stable manifold associated with $(\mathbf{q}_0,\mathbf{p}_0)_a$. With these heteroclinic orbits as reference trajectories, the neighboring orbits are well approximated by linearizing the local equations of motion. Although the linearization is only locally valid, the integration with ρ_a serves very effective to cut off this domain. There may be a particular trajectory within each branch which is optimal for use as the reference trajectory and which is not the heteroclinic orbit we are using. However, the contribution from each branch should depend only very weakly on the choice of orbit as long as it is coming from the heart of the branch and is not an orbit on the extreme fringe. The expression for $\mathscr{C}_{ab}(t)$ is reduced to a sum over contributions, one from each subset, γ:

$$\mathscr{C}_{ab}(t) \approx \sum_{\gamma} \langle \rho_a \rho_b(t) \rangle_{\gamma}. \tag{21}$$

Technically speaking, this is a sum of contributions over the numerous heteroclinic excursions. The result depends only on the parameters describing each excursion and the local stability of the dynamics. One complicating feature of Eq. (21) is that the orbits represented by γ depend on t. In principle, the sum is completely different for every t for which it is evaluated and the number of contributions will increase exponentially with time. However, it is still far easier to find the γ orbits than to perform the cellular dynamics.

C. The semiclassical version

Returning now to the quantum correlation function of Eq. (19), inserting $G_{sc}(\mathbf{q},\mathbf{q}';t)$ and following the reasoning above yields the approximation

$$C_{ab}(t) \approx \sum_{\gamma} \langle \Phi_a(0) | \Phi_b(t) \rangle_{\gamma}, \tag{22}$$

where for each γ in the sum, the overlap depends on a particular heteroclinic orbit and its environs. All the "nonlinearities" now reside in the summation. The local linearization amounts to Taylor expanding the action $S_j(\mathbf{q},\mathbf{q}';t)$ that appears in $G_{sc}(\mathbf{q},\mathbf{q}';t)$ to quadratic order in $\mathbf{q}$ and $\mathbf{q}'$ and evaluating the determinant prefactor (which is locally constant). In this way, only elementary Gaussian integrals (which are done analytically) are encountered in evaluating Eq. (19) semiclassically. We leave out the analytic expressions because they do not seem to be very enlightening. Again, though the linearized $S_j(\mathbf{q},\mathbf{q}';t)$ is valid only in a small neighborhood around its reference trajectory, the integral with $\Phi_a(\mathbf{q})$ serves to cut it off. Reference 18 gives a thorough summary of such linear wave packet dynamics. There is one slight twist here as compared to Ref. 18 since our reference trajectories do not lie at the center of the wave packet, but that is all. There are clear, strong similarities between stationary phase and our evaluation of Eq. (22); there are the Gaussian integrals, the linearization, the discrete final sum, etc. The precise connection is still under study.

D. Breaking the log time barrier in the stadium

A good testing ground of the semiclassical dynamics is provided by the well-studied quantized stadium billiard. The classical stadium is proven chaotic (highly unstable), and there is every reason to believe that the semiclassical dynamics should function in a way typical of many chaotic systems. If a localized wave packet of the form given in Eq. (5) is propagated, it will very rapidly spread to fill the entire stadium. For example, in Fig. 9 are the contours of the real part of a wave packet initially located at the center of the stadium moving toward the right. Scaling the time for the wave packet's horizontal traversal of the stadium to be $t=1$, the propagated wave function is shown for $t=0,1,2,6$. By $t=3$, the time of the shortest unstable periodic orbit, the wave function has already passed the "Ehrenfest time," i.e., it is barely recognizable as having originated from a localized state. Any obvious quantum-classical correspondence has already passed.

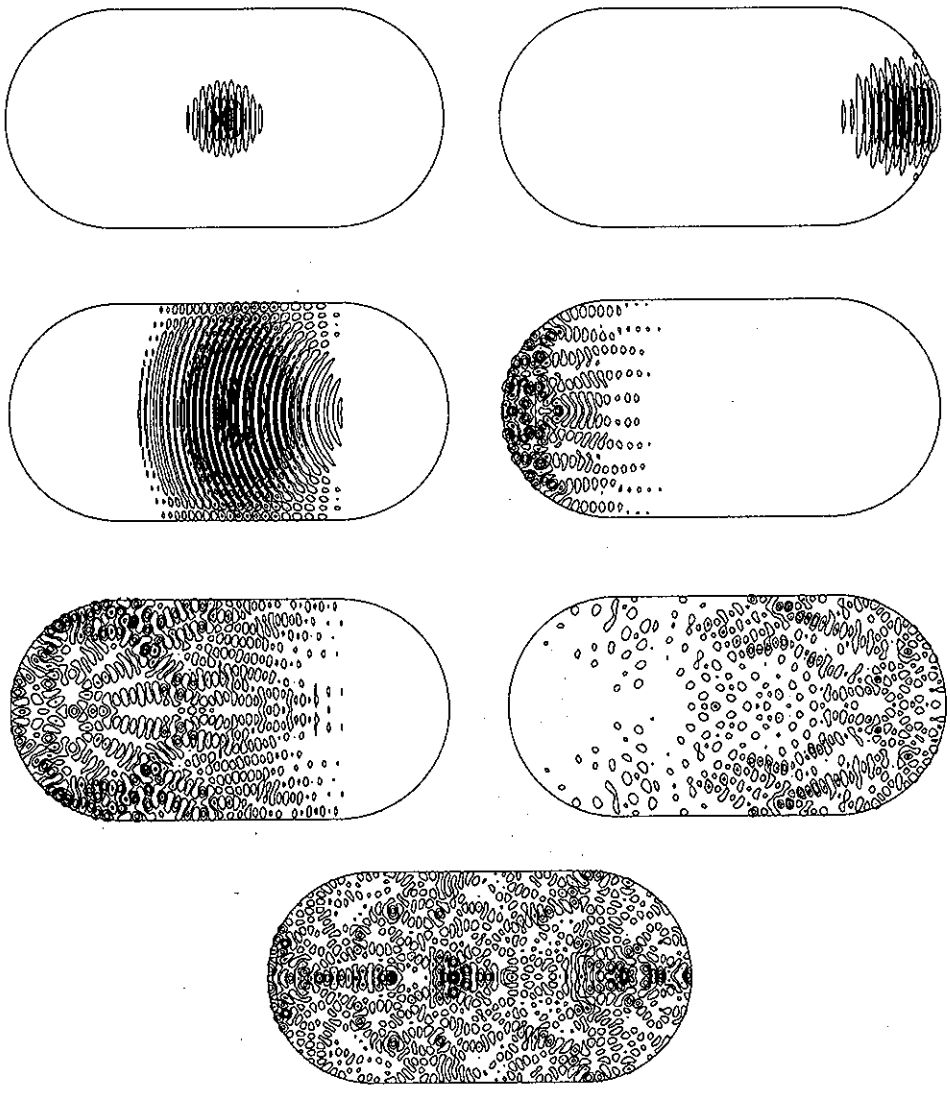

FIG. 9. Evolution of a localized wave packet in the stadium billiard. The initial Gaussian pictured in the first frame is chosen so that 30 wavelengths stretch across the horizontal axis.

The stadium has a few features that simplify the semiclassics and a few quirks. First, the trajectories remain geometrically the same as the energy is changed. This allows the γ summation to be interpreted as a sum over the geometric orbits ($\|\mathbf{p}\| = 1$) and to have a "free particle dynamics" to account for the actual momentum along the orbit as well as its uncertainty; all the orbits that follow a geometric path but with various momenta can be treated as a single orbit. Next, the boundary perimeter and parallel momentum serve as surface of section variables and give a convenient "bounce mapping" that simplifies generating the dynamics. All the γ orbits can be located working strictly from this surface of section. With minor adjustments, one also has all the $S_j(\mathbf{q},\mathbf{q}';t)$ and their stabilities as well.

Finally, the ν_j index has two components. A phase shift of $-\pi/2$ for each focal point and a phase shift for each bounce off a wall. Because there is only free particle motion between bounces, the focal point count can be reduced to observing the sign of one particular monodromy matrix element from bounce to bounce. The second component, due to the phase shift from bouncing off the walls, is more involved. For numerical reasons, our quantum calculations involve "soft" walls (sharp walls of finite height) in the time domain and hard walls (infinite height) in the energy domain. The bounce phase shift is $-\pi$ in the latter case and more complicated in the former. Other than to say the appropriate "bounce" phases are also put into the semiclassical approximation, we leave out all the details.

To give a quantitative semiclassical-quantum comparison, consider the autocorrelation function, $C_{bb}(t) = \langle \Phi_b(0) | \Phi_b(t) \rangle$, where $\Phi_b(0)$ is pictured in Fig. 9 at $t = 0$. The gross behavior of $C_{bb}(t)$ is easily understood. Its magnitude will begin at one and drop to nearly zero as the propagated wave packet begins to move away. It will remain nearly zero until $t \approx 2$ when parts of the wave packet will have had the time to travel back and forth across the stadium and generate partial recurrences. Soon thereafter, the quantum propagated state seems to be everywhere and $C_{bb}(t)$ will settle into some fluctuating pattern. This is borne out in Fig. 10(a) by the dashed (exact quantum) curve. The surprise is that every detail of the fluctuating quantum behavior is captured by the semiclassical prediction, which is superposed on the same figure as a solid

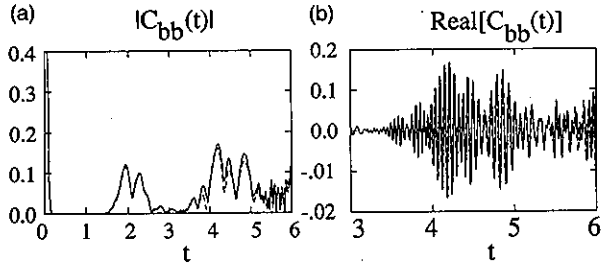

FIG. 10. The comparison of an exact quantum and a semiclassical calculation of an autocorrelation function. The quantum curves are dashed and the semiclassical are solid. In (a), the absolute magnitude of $C_{ab}(t)$ is plotted. In (b), a blowup is given of the real part of $C_{bb}(t)$.

curve. In Fig. 10(b), just the real part of $C_{bb}(t)$ is shown on an expanded scale to display better the quality of agreement. We have checked other cases, including examples with far fewer nodes, i.e., lower energies, (and cross correlations, $a \neq b$) and found similar agreement.

In performing the heteroclinic (homoclinic for autocorrelation functions) summation to obtain the semiclassical prediction, about a dozen orbits were contributing at any given time near $t \approx 2$. By $t \approx 4$, several hundred were contributing, and, by $t \approx 5$ or 6, more than 30 000 heteroclinic terms were needed in the summation. To picture the dynamical complexity, consider the bottom right image of Fig. 8, which shows seven branches slicing through the gray disk. To attain $t \approx 5$ or 6, one would have to draw more than 30 000 branches fitting in the gray disk. Other than for the beginning of the first recurrence, no individual orbit comes anywhere close to generating the magnitudes of the recurrences seen; all of the terms are necessary. In Fig. 11 is a segment of an important homoclinic orbit and its contribution $\langle \Phi_a(0) | \Phi_b(t) \rangle_\gamma$. Note that the scale of its magnitude is much smaller than found in the full sum pictured in Fig. 11.

Because our method approximates $G_{sc}(\mathbf{q},\mathbf{q}';t)$, the already quantitative results could only improve if a better evaluation of the semiclassical dynamics were available. Thus the intricate dynamics of chaotic motion do not have the strong adverse effect on the fundamental semiclassical approximation that had been believed.[10] Nearly all the thousands of branches of trajectories are *individually* generating accurate contributions to $C_{ab}(t)$; nearby branches do not compromise the accuracy of a given branch.

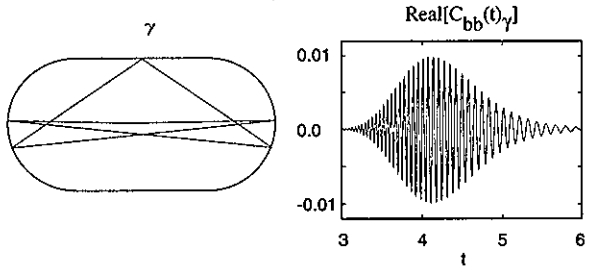

FIG. 11. A segment of an important homoclinic orbit (the part showing the excursion from the horizontal periodic orbit) and its contribution to the correlation function.

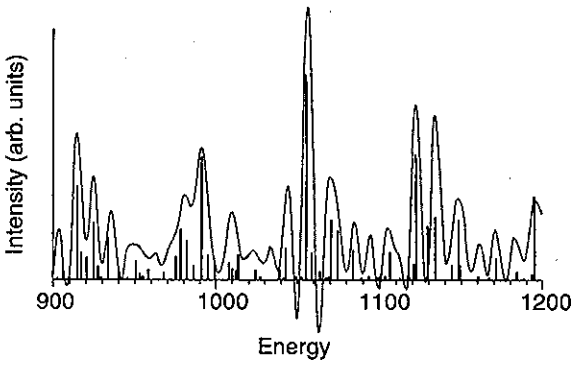

FIG. 12. The time-energy Fourier transform of $C_{bb}(t)$ (grey line) and exact spectrum of Φ_b. The transform is cutoff abruptly at $t = 8$ beyond which the number of heteroclinic orbits becomes impractical. For clarity, only the center third of the Φ_b spectrum is shown.

The overlap intensity of Φ_b with the eigenstates may be obtained by Fourier transforming the dynamics. Figure 12 shows the comparison of the transformed semiclassics with the exact quantum intensity spectrum. The maximum peak occurs near the 1 200th eigenvalue. Remarkably, the semiclassical theory is reproducing the quantum fine structure to the scale of two to three mean spacings. The limit of resolution results from the present practical limit of performing the classical dynamics and not by any failure of the semiclassics. The ability to resolve structure on the scale of an average spacing or less has been a major goal since efforts began on understanding the semiclassical dynamics of chaos.

IV. CONCLUSIONS

There are many physical phenomena which are best calculated in the time domain: Whenever the "essential physics" is short time. This holds true even if the formalism is traditionally cast in the energy domain. Examples include many types of particle scattering, absorption and Raman spectroscopy, and pulsed laser experiments. For this reason alone, a good semiclassical propagator is needed. Even if one is interested in energy domain explicitly, it is available from the time domain by Fourier transform.

We have shown that the venerable Van Vleck Green's function, which is the fundamental semiclassical object in the time domain, is remarkably computable and remarkably accurate. It seems that the lack of attention devoted to the Van Vleck Green's function resulted from too pessimistic a prognosis of its utility and accuracy. To this, one must add the ever present bias against the time domain where pure state quantum mechanics is concerned, a bias which is now rapidly dissipating.

Although some of the gloomy predictions were without foundation, others are based on apparently sound ideas, which leave us still a bit astonished about the accuracy we are finding, especially in the chaotic regime. Sim-

ilar accuracy and conclusions were also reached in the aforementioned work on the quantum baker's map.[19]

We should not leave the impression that the Van Vleck Green's function is infallible or that it will not break down. There is no doubt that diffractive effects are completely absent from the primitive (nonuniformized) methods we have described here. Apart from the obvious nonclassical diffraction one gets behind a sharp barrier, more subtle effects responsible for quantum tunneling or quantum localization may be due to diffraction. As an example, consider the branches for which our technique of evaluating Eq. (3) must break down, i.e., those folded within the overlap region. In the stadium, a fold develops when one of the local trajectories strikes the joint between the semicircular endcap and the straight edge. These folds generate sources of diffraction and that is certainly left out of Eq. (3).

We cannot help but be excited by these results, because the realm of potential applicability is so large (after all, we are talking about the fundamental quantum propagator!), and because there is so much to do to understand these new aspects of semiclassical approximation. We need no longer be concerned that classical chaos puts semiclassical methods out of business. This conclusion, reached here through the time domain, is paralleled by the beautiful energy domain results which were presented by several groups at the Copenhagen meeting, and which are described in this issue of Chaos.

There are several natural continuations of this work that we are pursuing. Examples include: (i) understanding better the domain of time and $\hbar$ in which semiclassical arguments are valid; (ii) searching ways of summarizing the classical information in order to simplify evaluating the heteroclinic summation; (iii) investigating the nature of "chaotic" eigenfunctions incorporating the newfound access to long time dynamics; (iv) re-examining Gutzwiller periodic orbit theory for possible corrections and new insight; and (v) further development of the semiclassical techniques for application to physical systems.

ACKNOWLEDGMENTS

We acknowledge fruitful discussions with P. W. O'Connor and R. Legere. This research was supported by the National Science Foundation under Grant No. CHE-9014555. One of us (MAS) acknowledges support from the Ministerio de Educación y Ciencia of Spain.

[1] J. H. Van Vleck, Proc. Natl. Acad. Sci. USA **14**, 178 (1928).
[2] V. P. Maslov and M. V. Fedoriuk, *Semiclassical Approximations in Quantum Mechanics* (Reidel, Dordrecht, The Netherlands, 1981), English translation.
[3] M. C. Gutzwiller, J. Math. Phys. **12**, 343 (1971), and references therein.
[4] M. V. Berry and N. L. Balazs, J. Phys. A **12**, 625 (1979); M. V. Berry, N. L. Balazs, M. Tabor, and A. Voros, Ann. Phys. (NY) **122**, 26 (1979).
[5] Z. V. Lewis, "Quantizing fine scale classical structure," Ph.D. thesis, University of Bristol, 1982; see also M. V. Berry, Ann. NY Acad. Sci. **357**, 183 (1982).
[6] M. C. Gutzwiller, Physica D **5**, 183 (1982).
[7] E. B. Bogomolny, Physica D **31**, 169 (1988).
[8] A. M. Ozorio de Almeida, *Nonlinearity* **2**, 519 (1989).
[9] M. Sieber and F. Steiner, Physica D **44**, 248 (1990); some very recent advances hold much promise, see, for example, G. Tanner, P. Scherer, E. B. Bogomolny, B. Eckhardt, and D. Wintgen, Preprint.
[10] A. Voros, J. Phys. A: Math. Gen. **21**, 685 (1988).
[11] E. J. Heller, Phys. Rev. Lett. **53**, 1515 (1984).
[12] E. J. Heller, J. Chem. Phys. **24** (4), 2723 (1991).
[13] M. Sepúlveda and E. J. Heller, Preprint.
[14] S. Tomsovic and E. J. Heller, Phys. Rev. Lett. **67**, 664 (1991).
[15] [a]W. H. Miller, J. Chem. Phys. **53**, 1949, 3578 (1970); [b]W. H. Miller, Adv. Chem. Phys. **25**, 69 (1974).
[16] D. Huber, E. J. Heller, and R. G. Littlejohn, J. Chem. Phys. **89** (4), 2003 (1988).
[17] E. J. Heller, J. Chem. Phys. **67**, 3339 (1977).
[18] E. J. Heller, "Wavepacket dynamics and quantum chaology," in *Chaos and Quantum Physics*, edited by M. J. Giannoni, A. Voros, and J. Zinn-Justin (Elsevier, Amsterdam, 1990).
[19] Patrick W. O'Connor, Steven Tomsovic, and Eric J. Heller, Physica D (in press).
[20] Steven Tomsovic and Eric J. Heller (in preparation).